
Cross-Model Consensus of Explanations and Beyond for Image Classification Models: An Empirical Study

Xuhong Li

Baidu Research, Baidu Inc
lixuhong@baidu.com

Haoyi Xiong

Baidu Research, Baidu Inc
xionghaoyi@baidu.com

Siyu Huang

Nanyang Technological University
siyu.huang@ntu.edu.sg

Shilei Ji

Baidu Inc
jishilei@baidu.com

Dejing Dou

Baidu Research, Baidu Inc
doudejing@baidu.com

Abstract

Existing interpretation algorithms have found that, even deep models make the same and right predictions on the same image, they might rely on different sets of input features for classification. However, among these sets of features, some common features might be used by the majority of models. In this paper, *we are wondering what are the common features used by various models for classification and whether the models with better performance may favor those common features*. For this purpose, our works uses an interpretation algorithm to attribute the importance of features (e.g., pixels or superpixels) as explanations, and proposes the *cross-model consensus of explanations* to capture the common features. Specifically, we first prepare a set of deep models as a *committee*, then deduce the explanation for every model, and obtain the *consensus* of explanations across the entire committee through *voting*. With the cross-model consensus of explanations, we conduct extensive experiments using 80+ models on 5 datasets/tasks. We find three interesting phenomena as follows: (1) the consensus obtained from image classification models is aligned with the ground truth of semantic segmentation; (2) we measure the similarity of the explanation result of each model in the committee to the consensus (namely *consensus score*), and find positive correlations between the consensus score and model performance; and (3) the consensus score coincidentally correlates to the interpretability.

1 Introduction

Deep models are well-known by their excellent performance in many challenging domains, as well as their black-box nature. To interpret the prediction of a deep model, a number of trustworthy interpretation algorithms [4, 59, 37, 44, 45, 31] have been recently proposed to attribute the importance of every input feature in a given sample with respect to the model’s output. For example, given an image classification model, LIME [37] and SmoothGrad [44] could attribute the importance scores to every superpixel/pixel in an image with respect to the model’s prediction. In this way, one can easily explain the classification result of a model with a data point by visualizing the important features used by the model for prediction.

The use of interpretation tools finds that, even deep models make the same and right predictions on the same image, they might rely on different sets of input features for classification. For example, our work uses LIME and SmoothGrad to explain a number of models trained on image classification tasks on the same set of images and obtains different explanations for these models even all they make right predictions (latterly shown in Figure 2 and Figure 3). While these models have been

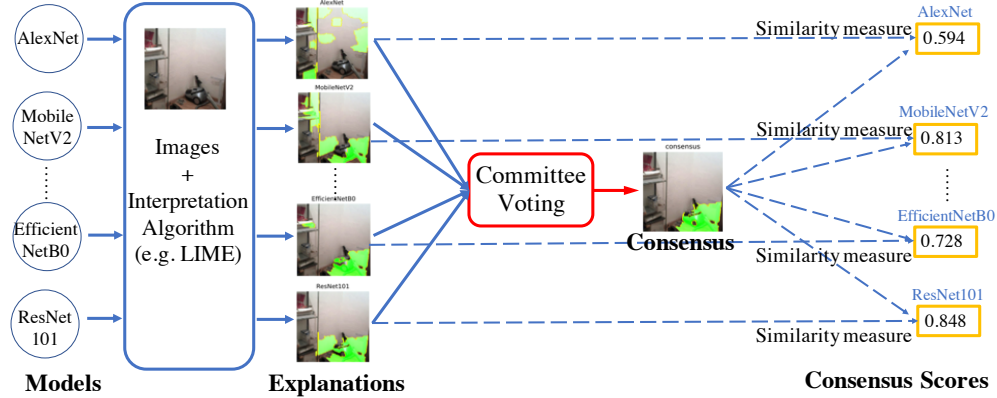


Figure 1: Illustration of the proposed framework that consists of the three steps: (1) prepares a set of trained models as committee, (2) aggregates explanation results across the committee to get the consensus, and (3) computes the similarity score of each explanation to the consensus.

explained to make the same prediction using different sets of features, we can still find that some common features might be used by the majority of models. In this way, we are particularly interested in two research questions as follows: (1) *What are the common features used by various models in an image?* (2) *Whether the models with better performance favor those common features?*

To answer these two questions, we propose to study the common features across a number of deep models and measure the similarity between the set of common features and the one used by every single model. Specifically, as illustrated in Figure 1, we generalize an electoral system to first form a *committee* with a number of deep models, then obtain the explanations for a given image based on one trustworthy interpretation algorithm, then call for *voting* to obtain the *cross-model consensus of explanations*, or shortly *consensus*, and finally compute a similarity score between the consensus and the explanation result for each deep model, denoted as *consensus score*. Through extensive experiments using 80+ models on 5 datasets/tasks, we find that (1) the consensus is aligned with the ground truth of image semantic segmentation; (2) a model in the committee with a higher consensus score usually performs better in terms of testing accuracy; and (3) models’ consensus scores coincidentally correlates to their interpretability.

The contributions of this paper could be summarized as follows. To the best of our knowledge, this work is the first to investigate the common features, which are used and shared by a large number of deep models for image classification, by incorporating with interpretation algorithms. We propose the cross-model consensus of explanations to characterize the common features, and connect the consensus score to the performance and interpretability of a model. Finally, we obtain three observations from the experiments with thorough analyses and discussions.

2 Related Work

We first review the interpretation algorithms and the evaluation approaches on their trustworthiness. To visualize the activated subregions of intermediate-layer feature maps, many algorithms have been proposed to interpret convolutional networks [59, 40, 7, 51]. Apart from investigating the inside of complex deep networks, simple linear or tree-based surrogate models have been used as “out-of-box explainers” to explain the predictions made by the deep model over the dataset through local or global approximations [37, 48, 2, 57]. Instead of using surrogates for deep models, algorithms, such as SmoothGrad [44], Integrated Gradients [45], DeepLIFT [42] etc, have been proposed to estimate the input feature importance with respect to the model predictions. Note that there are many other interpretation algorithms and we mainly discuss the ones that are related to feature attributions and suitable for deep models for image classification in this paper. Evaluations on the trustworthiness of interpretation algorithms are of objective to qualify their trustworthiness and not mislead the understanding of models’ behaviors, e.g. Adebayo et al. [1] have found that some algorithms are independent both of the model and the data generating process, through randomizing the parameters of models. Other evaluation approaches include perturbation of important features [38, 34, 50, 17],

model trojanning attacks [8, 15, 29], infidelity and sensitivity [3, 56] to similarity samples in the neighborhood, through a crafted dataset [55], and user-study experiments [27, 23].

From an orthogonal perspective, evaluations across models are also urged for building more interpretable and explainable AI systems. However, evaluations across the deep models are scarce. Bau et al. [5] proposed *Network Dissection* to build an additional dataset with dense annotations of a number of visual concepts for evaluating the interpretability of convolutional neural networks. Given a convolutional model, Network Dissection recovers the intermediate-layer feature maps used by the model for the classification, and then measures the overlap between the activated subregions in the feature maps with the densely human-labeled visual concepts to estimate the interpretability of the model. Another common solution to the evaluation across deep models is user-study experiments [13].

In this paper, we do not directly evaluate the interpretability across deep models, but based on the proposed framework, we show experimentally that the consensus score is positively correlated to the generalization performance of deep models and coincidentally related to the interpretability. We will discuss more details with analyses later. We believe that based on the explanations, our proposed framework and the consensus score could help to better understand deep models.

3 Framework of Cross-Model Consensus of Explanations

In this section, we introduce the proposed approach that generalizes the electoral system to provide the consensus of explanations across various deep models. Specifically, the proposed framework consists of three steps, as detailed in the following.

Step1: Committee Formation with Deep Models. Given m deep models that are trained for solving a target task (image classification task in our experiments) on a visual dataset where each image contains one main object, the approach first forms the given deep models as a *committee*, noted as \mathcal{M} , and then considers the variety of models in the committee that would establish the consensus for comparisons and evaluations.

Step2: Committee Voting for Consensus Achievement. With the committee of deep models and the task for explanation, the proposed framework leverages a trustworthy interpretation tool \mathcal{A} , e.g. we choose LIME [37] or SmoothGrad [44] as \mathcal{A} in this paper, to obtain the explanation of every model on every image in the dataset. Given some sample d_i from the dataset, we note the obtained explanation results of all models as \mathbf{L} . Then, we propose a *voting* procedure that aggregates \mathbf{L} to reach the cross-model consensus of explanations, i.e., the *consensus*, \mathbf{c} for d_i . Specifically, the k -th element of the consensus \mathbf{c} is $c_k = \frac{1}{m} \frac{\sum_{i=1}^m L_{ik}^2}{\|\mathbf{L}_i\|}$, $\forall 1 \leq k \leq K$ for LIME, where K

refers to the dimension of an explanation result and $c_k = \frac{1}{m} \sum_{i=1}^m \frac{L_{ik} - \min(\mathbf{L}_i)}{\max(\mathbf{L}_i) - \min(\mathbf{L}_i)}$, $\forall 1 \leq k \leq K$ for SmoothGrad, following the conventional normalization-averaging procedure [37, 2, 44]. To the end, the consensus has been reached for every sample in the target dataset based on committee voting.

Step3: Consensus-based Similarity Score. Given the consensus, the approach calculates the *consensus score* of every model in the committee by considering the similarity between the explanation result of each individual model and the consensus. Specifically, for the explanations and the consensus based on LIME (visual feature importance in superpixel levels), cosine similarity between the flattened vector of explanation of each model and the consensus is used. For the results based on SmoothGrad (visual feature importance in pixel levels), a similar procedure is followed, where the proposed algorithm uses Radial Basis Function ($\exp(-\frac{1}{2}(\|\mathbf{a} - \mathbf{b}\|/\sigma)^2)$) for the similarity mea-

Algorithm 1: Framework Pseudocode.

```

1 Input: A dataset  $\mathcal{D}$  and an interpretation algorithm  $\mathcal{A}$ .
  /* Step 1: Committee Formation with Deep Models */
2 Train  $m$  deep models on  $\mathcal{D}$  that form the committee  $\mathcal{M}$ .
  /* Step 2: Committee Voting for Consensus Achievement */
3 For each example  $d_i$  in  $\mathcal{D}$ , initialize an empty matrix  $\mathbf{L}$  for storing the explanations.
4 for each model  $M_j$  in  $\mathcal{M}$  do
5   |  $\mathbf{L}_j = \text{interpret}(\mathcal{A}, d_i, M_j)$ 
6 end
7  $\mathbf{c} = \text{reach\_consensus}(\mathbf{L})$ 
  /* Step 3: Consensus-based Similarity Score */
8 for each model  $M_j$  in  $\mathcal{M}$  do
9   |  $s_j = \text{similarity}(\mathbf{L}_j, \mathbf{c})$  as the score of  $M_j$  for  $d_i$ .
10 end
11 Repeat Step2 and Step3 for all examples in  $\mathcal{D}$ . For each model  $M_j$ , the overall consensus score is the average of the similarity scores over all examples.
```

surement. The difference in similarity computations is due to that (1) the dimensions of LIME explanations are various for different samples while invariant for SmoothGrad explanations; (2) the scales of LIME explanation results vary much larger than SmoothGrad. Thus cosine similarity is more suitable for LIME while RBF is for SmoothGrad. Eventually, the framework computes a quantitative but relative score for each model in the committee using their similarity to the consensus.

For further clarity, these three steps of the proposed framework are illustrated in Figure 1 and formalized in Algorithm 1, with more details in the appendix.

4 Overall Experiments and Results

In this section, we start by introducing the experiment setups. We use the image classification as the target task and follow the proposed framework to obtain the consensus and compute the consensus scores. Through the experiments, we have found (1) the alignment between the consensus and image semantic segmentation, (2) positive correlations between the consensus score and model performance, and (3) coincidental correlations between the consensus score and model interpretability. We end this section by robustness analyses of the framework.

4.1 Evaluation Setups

Datasets. For overall evaluations and comparisons, we use ImageNet [11] for general visual object recognition and CUB-200-2011 [53] for bird recognition respectively. Note that ImageNet provides the class label for every image, and the CUB-200-2011 dataset includes the class label and pixel-level segmentation for the bird in every image, where the pixel annotations of visual objects are found to be aligned with the consensus.

Models. For fair comparisons, we use more than 80 deep models trained on ImageNet that are publicly available¹. We also derive models on the CUB-200-2011 dataset through standard fine-tuning procedures. In our experiments, we include these models of the two committees based on ImageNet and CUB-200-2011 respectively. Both of them target at the *image classification* task with each image being labeled to one category.

Interpretation Algorithms. As we previously introduced, we consider two interpretation algorithms, LIME [37] and SmoothGrad [44]. Specifically, LIME surrogates the explanation as the assignment of visual feature importance to superpixels [49], and SmoothGrad outputs the explanations as the visual feature importance over pixels. In this way, we can validate the flexibility of the proposed framework over explanation results from diverse sources (i.e., linear surrogates vs. input gradients) and in multiple granularity (i.e., feature importance in superpixel/pixel-levels).

4.2 Alignment between the Consensus and Image Segmentation

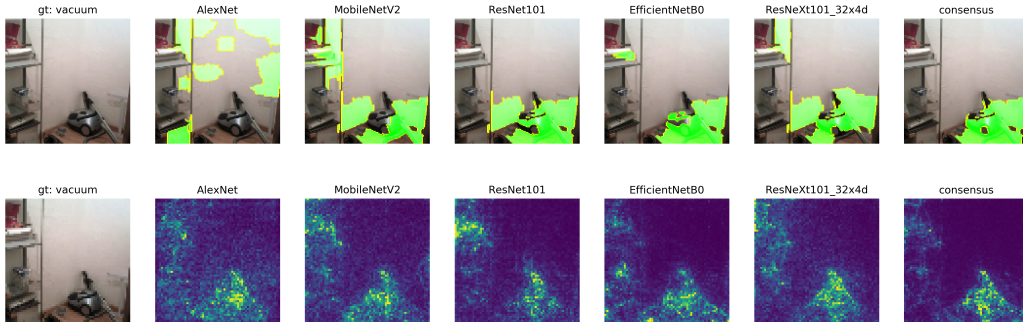


Figure 2: Visual comparisons between consensus and the interpretation results of CNNs using LIME (in the upper line) and SmoothGrad (in the lower line) based on an image from ImageNet, where the ground truth of segmentation is not available.

¹https://github.com/PaddlePaddle/models/blob/release/1.8/PaddleCV/image_classification/README_en.md#supported-models-and-performances

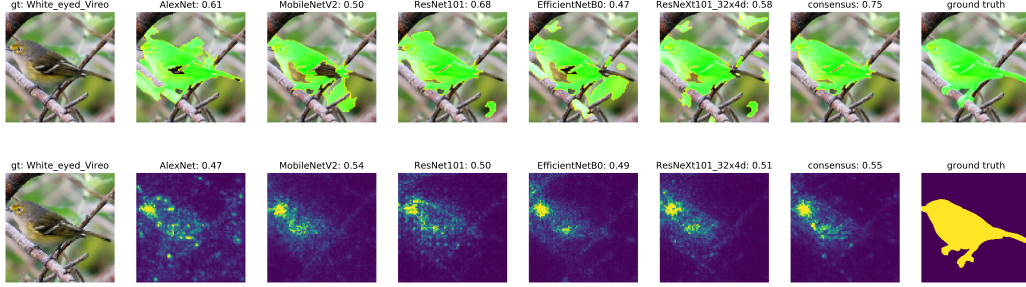


Figure 3: Visual comparisons between consensus and the explanation results of deep models using LIME (in the upper line) and SmoothGrad (in the lower line) based on an image from CUB-200-2011, where the ground truth of segmentation is available as pixel-wise annotations and the mean Average Precision (mAP) are measured.

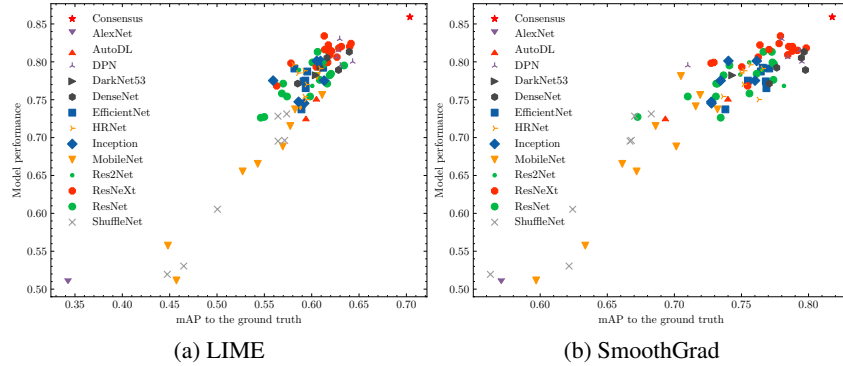


Figure 4: Correlation between model performance and mAP to the segmentation ground truth using (a) LIME and (b) SmoothGrad with CUB-200-2011 over 85 models. Pearson correlation coefficients are 0.927 (with p-value $4e-37$) for LIME and 0.916 (with p-value $9e-35$) for SmoothGrad. The points “Consensus” here refer to the testing accuracy of the ensemble of networks in the committee by probabilities averaging and voting (in y-axis), as well as the mAP between the consensus and the ground truth (in x-axis).

The image segmentation task searches the pixel-wise classifications of images. Cross-model consensus of explanations for image classification are well aligned to image segmentation, especially when only one main object is contained in the image. This partially demonstrates the effectiveness of most deep models in extracting visual objects from input images. We show two examples using both LIME and SmoothGrad in Figure 2 and 3 from ImageNet and CUB-200-2011 respectively. More examples can be found in appendix.

To quantitatively demonstrate the alignment, we compute the Average Precision (AP) score between the cross-model consensus of explanations and the image segmentation ground truth on CUB-200-2011, where the latter is available. We further take the mean of AP scores (mAP) over the dataset to compare with the overall consensus scores. Figure 4 shows the results, where the consensus achieves higher mAP scores than any individual network. Both quantitative results and visual comparisons in validate the closeness of consensus to the ground truth of image segmentation.

4.3 Positive Correlations between Consensus Scores and Model Performance

Figure 5 shows the positive correlations between the similarity score to the consensus (in x-axis) and model performance (in y-axis). Specifically, in Figure 5 (a-b) and (d-e), we present the results using LIME (a,d) and SmoothGrad (b,e) on ImageNet (a,b) and CUB-200-2011 (d,e). All correlations here are strong with significance tests passed, though in some local areas of the correlation plots between the consensus score and model performance. In this way, we could conclude that, in an overall manner, the evaluation results based on the consensus score using both LIME and SmoothGrad over

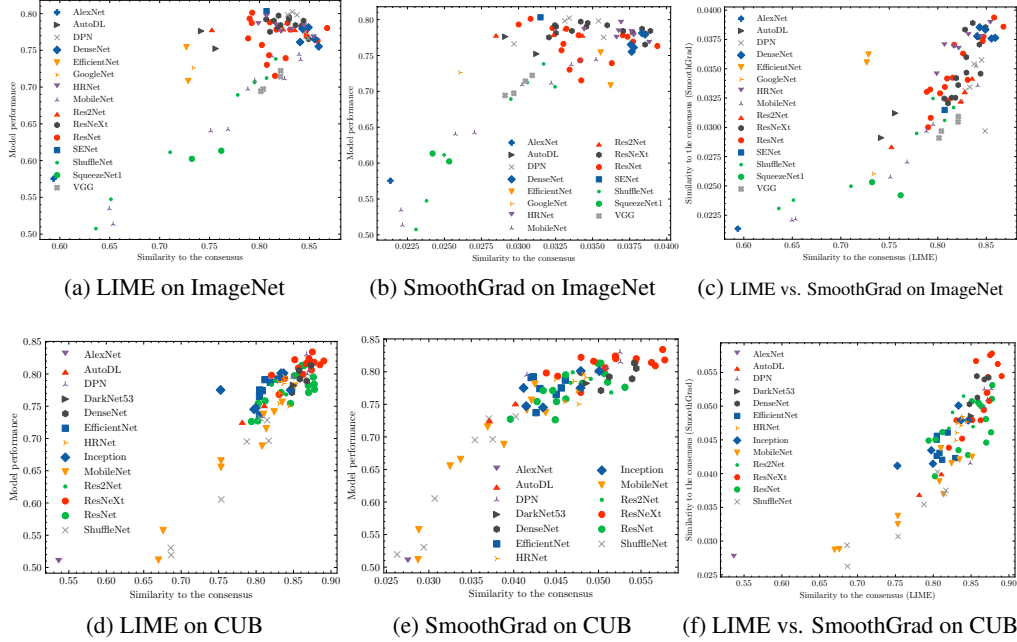


Figure 5: Model performance v.s. similarity to the consensus using LIME (a,d) and SmoothGrad (b,e) over 81 models on ImageNet (a,b) and 85 models on CUB-200-2011 (d,e). The third column shows the similarity to the consensus of SmoothGrad interpretations v.s. similarity to the consensus of LIME interpretations on ImageNet committee (c) and CUB-200-2011 committee (f). Pearson correlation coefficients are (a) 0.8087, (b) 0.783, (c) 0.825, (d) 0.908, (e) 0.880 and (f) 0.854. For concise purpose, networks in the same family are represented by the same symbol.

Table 1: Rankings (and scores) of five deep models, evaluated by Network Dissection [5], user-study evaluations, and the proposed framework with LIME and SmoothGrad.

	DenseNet161	ResNet152	VGG16	GoogleNet	AlexNet
Network Dissection	2	1	3	4	5
User-Study Evaluations	1 (1.715)	2 (1.625)	3 (1.585)	4 (1.170)	5 (0.840)
Consensus (LIME)	1 (0.849)	2 (0.846)	3 (0.821)	4 (0.734)	5 (0.594)
Consensus (SmoothGrad)	1 (0.038)	2 (0.037)	3 (0.030)	4 (0.026)	5 (0.021)

the two datasets are correlated to model performance with significance. More experiments on other datasets with random subsets of deep models will be shown in in Figure 7 (Section 4.5).

4.4 “Coincidental” Correlations between Consensus Scores and Model Interpretability

Deep model interpretability measures *the ability to present in understandable terms to a human* [13]. While no formal and agreed measurements for the interpretability evaluation, two evaluation methods, i.e., Network Dissection [5] and user-study experiments, are quite common for this purpose. Though the proposed framework and the consensus scores are based on explanation results, they do not directly estimate the model interpretability. Nevertheless, in this subsection, we present the coincidental correlations between the consensus scores and the interpretability measurements.

Consensus versus Network Dissection. We compare the results of the proposed framework with the interpretability evaluation solution Network Dissection [5]. On the Broden dataset, Network Dissection reported a ranking list of five models (w.r.t. the model interpretability), shown in Table 1, through counting the semantic neurons, where a neuron is defined *semantic* if its activated feature maps overlap with human-annotated visual concepts. Based on the proposed framework, we report the consensus scores of using LIME and SmoothGrad in Table 1, which are consistent to

Figure 5 (a, LIME) and (b, SmoothGrad). The three ranking lists are almost identical, except the comparisons between DenseNet161 and ResNet152, where in the both lists based on the consensus score, DenseNet161 is similar to ResNet152 with marginally elevated consensus scores, while Network Dissection considers ResNet152 is more interpretable than DenseNet161.

We believe the results from our proposed framework and Network Dissection are close enough from the perspectives of ranking lists. The difference may be caused by the different ways that our framework and Network Dissection perform the evaluations. The consensus score measures the similarity to the consensus explanations on images, while Network Dissection counts the number of neurons in the intermediate layers activated by all the visual concepts, including objects, object parts, colors, materials, textures and scenes. Furthermore, Network Dissection evaluates the interpretability of deep models using the Broden dataset with densely labeled visual objects and patterns [5], while the consensus score does not need additional datasets or the ground truth of semantics. In this way, the results by our proposed framework and Network Dissection might be slightly different.

Consensus versus User-Study Evaluations. In order to further validate the effectiveness of the proposed framework, we have also conducted user-study experiments on these five models and report the results on the second row of Table 1. See the appendix for the experimental settings of the user-study evaluations. This confirms that our proposed framework is capable of approximating the model interpretability.

4.5 Robustness Analyses of Consensus

In this subsection, we investigate several factors that might affect the evaluation results with consensus, including the use of basic interpretation algorithms (e.g., LIME and SmoothGrad), the size of committee, and the candidate pool for models in the committee.

Consistency between LIME and SmoothGrad. Even though the granularity of explanation results from LIME and SmoothGrad are different, which causes mismatching in mAP scores to segmentation ground truth, the consensus scores based on the two algorithms are generally consistent. The consistency has been confirmed by Figure 5 (c, f), where the overall results based on LIME is strongly correlated to SmoothGrad over all models on both datasets. This shows that the proposed framework can work well with a wide spectrum of basic interpretation algorithms.

Consistency of Cross-Committee Evaluations. In real-word applications, the committee-based estimations and evaluations may make inconsistent results in a committee-by-committee manner. In this work, we are interested in whether the consensus score estimations are consistent against the change of committee. Given 16 ResNet models as the targets, we form 20 independent committees through combining the 16 ResNet models with 10–20 models randomly drawn from the rest of networks. In each of these 20 independent committees, we compute the consensus scores of the 16 ResNet models. We then estimate the Pearson correlation coefficients between any of these 20 results and the one in Figure 5 (a), where the mean correlation coefficient is 0.96 with the standard deviation 0.04. Thus, we can say the consensus score evaluation would be consistent against randomly picked committees.

Convergence over Committee Sizes

To understand the effect of the committee size to the consensus score estimation, we run the proposed framework using committees of various sizes formed by deep models that are randomly picked up from the pools. In Figure 6, we plot and compare the performance of the consensus with increasing committee sizes, where we estimate the mAP between the ground truth and the consensus reached by the random committees of different sizes and 20 random trials have been done for every single size independently. It shows that the curve of mAP would

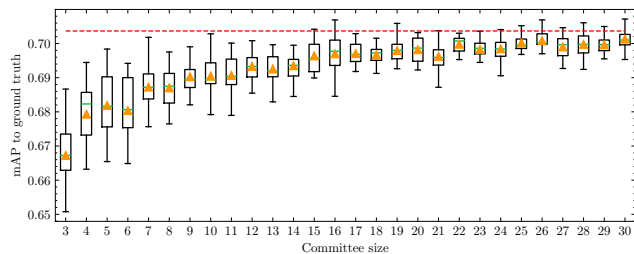


Figure 6: Convergence of mAP between the ground truth and the consensus results based on committees of increasing sizes, using LIME on CUB-200-2011. The green lines and orange triangles are, respectively, the mean values and the median values of 20 random trials. The red dashed line is the mAP of the consensus reached by the complete committee of the original 85 models.

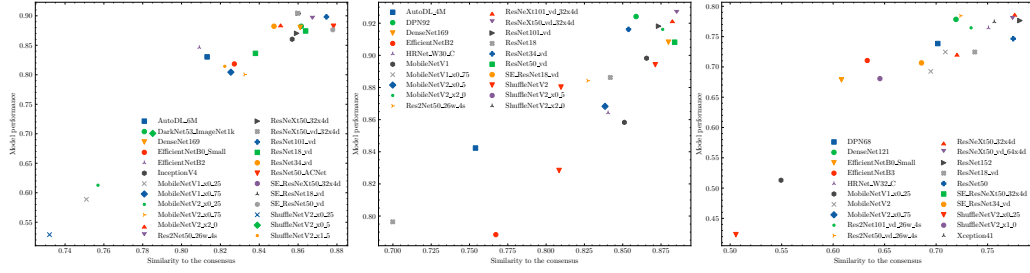


Figure 7: Model performance v.s. the consensus scores using LIME on Stanford Cars 196 [25], Oxford Flowers 102 [33] and Foods 101 [6]. Pearson correlation coefficients are 0.9522, 0.8785 and 0.9134 respectively.

quickly converge to the complete committee, while the consensus based on a small proportion of committee (e.g., 15 networks) works good enough even compared to the complete committee of 85 networks.

Applicability with Random Committees over More Datasets. To demonstrate the applicability of the proposed framework, we extend our experiments using networks randomly picked up from the pool to other datasets, including Stanford Cars 196 [25], Oxford Flowers 102 [33] and Foods 101 [6]. Dataset descriptions and experimental details are included in the appendix. The results in Figure 7 confirm that the positive correlations between the consensus score and model performance exist for a wide range of models on ubiquitous datasets/tasks.

5 Discussions: Limits and Potentials with Future Works

Limits. In this section, we would like to discuss several limits in our studies. First of all, we propose to study the features used by deep models for classification, but we use the explanation results (i.e., importance of superpixels/pixels in the image for prediction) obtained by interpretation algorithms. Obviously, the correctness of interpretation algorithms might affect our results. However, we use two independent algorithms, including LIME [37] and SmoothGrad [44], which attribute feature importance in two different scales i.e., superpixels and pixels. Both algorithms lead to the same observations and conclusive results (see Section 4.5 for the consistency between results obtained by LIME and SmoothGrad). Thus, we believe the interpretation algorithms here are trustworthy and it is appropriate to use explanation results as a proxy to analyze features. For future research, we would include more advanced interpretation algorithms to confirm our observations.

We obtain some interesting observations from our experiments and make conclusions using multiple datasets. However, the image classification datasets used in our experiments have some limits — every image in the dataset only consists of one visual object for classification. It is reasonable to doubt that when multiple visual objects (rather than the target for classification) and complicated visual patterns for background [24, 8] co-exist in an image, the cross-model consensus of explanations may no longer overlap to the ground truth semantic segmentation. Actually, we include an example of COCO dataset [28] in appendix, where multiple objects co-exist in the image and consensus may not always match the segmentation. Our future work would focus on the datasets with multiple visual objects and complicated background for object detection, segmentation, and multi-label classification tasks.

Finally, only well-known models with good performance have been included in the committee. It certainly would bring some bias in our analysis. However, in practice, these models would be one of the first choices or frequently used in many applications for relevance. In our future work, we would include more models with diverse performance to seek more observations.

Potentials. In addition to the limits, our work also demonstrates several potentials of cross-model consensus of explanations for further studies. As was shown in Figure 6, with a larger committee, the consensus would slowly converge to a stable set of common features that clearly aligns with the segmentation ground truth of the dataset. This experiment further demonstrates the capacity

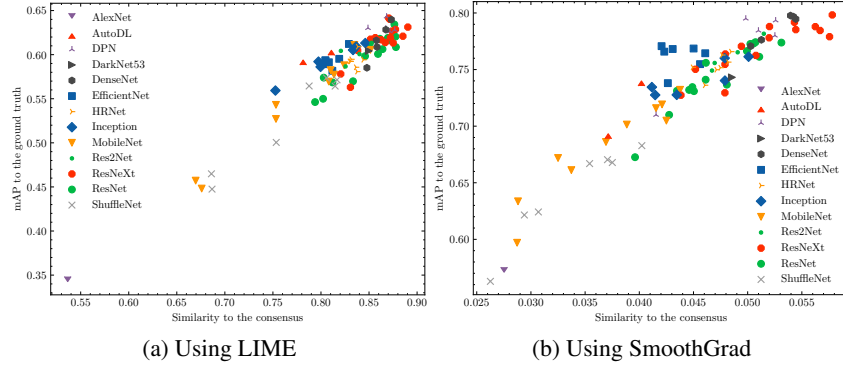


Figure 8: Correlation between mAP scores to the segmentation ground truth and the consensus scores using (a) LIME and (b) SmoothGrad with the CUB-200-2011 dataset over 85 models (of the committee). Pearson correlation coefficients are 0.885 (with p-value $3e-29$) for LIME and 0.906 (with p-value $8e-33$) for SmoothGrad.

of consensus to precisely position the visual objects for classification. Thus, in our future work, we would like to use consensus based on a committee of image classification models to detect the position of visual objects in the image.

Furthermore, our experiments with both interpretation algorithms on all datasets have found that consensus scores are “coincidentally” correlated to the interpretability scores of the models, even though interpretability scores were evaluated through totally different ways — network dissections [5] and user studies. Actually, network dissections evaluate the interpretability of a model through matching its activation maps in intermediate layers with the ground truth segmentation of visual concepts in the image. A model with higher interpretability should have more convolutional filters activated at the visual patterns/objects for classification. In this way, we particularly measure the similarity between the explanation results obtained for every model and the segmentation ground truth of images. We found that the models’ segmentation-explanation similarity significantly correlates to their consensus score (see Figure 8). This observation might encourage us to further study the connections between interpretability and consensus scores in the future work.

6 Conclusion

In this paper, we study the common features shared by various deep models for image classification. We are wondering (1) what are the common features and (2) whether the use of common features could improve the performance. Specifically, given the explanation results obtained by interpretation algorithms, we propose to aggregate the explanation results from different models, and obtain the cross-model consensus of explanations through voting. To understand features used by every model and the common ones, we measure the consensus score as the similarity between the consensus and the explanation of every model.

Our empirical studies based on extensive experiments using 80+ deep models on 5 datasets/tasks find that (i) the consensus aligns with the ground truth semantic segmentation of the visual objects for classification; (ii) models with higher consensus scores would enjoy better testing accuracy; and (iii) the consensus scores coincidentally correlate to the interpretability scores obtained by network dissections and user evaluations. In addition to main claims, we also include additional experiments to demonstrate robustness of consensus, including the alternative use of LIME and SmoothGrad and their effects to the results/conclusions, consistency of consensus achieved by different groups of deep models, the fast convergence of consensus with increasing number of deep models in the committee, and random selection of deep models as the committee for consensus-based evaluation on the other datasets. All these studies confirm the applicability of consensus as a proxy to study and analyze the common features shared by different models in our research. Several open issues and potentials have been discussed with future directions introduced. Hereby, we are encouraged to further adopt consensus and consensus scores to understand the behaviors of deep models better.

References

- [1] Adebayo, J., Gilmer, J., Muelly, M., Goodfellow, I., Hardt, M., and Kim, B. Sanity checks for saliency maps. In *Advances in Neural Information Processing Systems (NeurIPS)*, pp. 9505–9515, 2018.
- [2] Ahern, I., Noack, A., Guzman-Nateras, L., Dou, D., Li, B., and Huan, J. Normlime: A new feature importance metric for explaining deep neural networks. *arXiv preprint arXiv:1909.04200*, 2019.
- [3] Ancona, M., Ceolini, E., Öztireli, C., and Gross, M. Towards better understanding of gradient-based attribution methods for deep neural networks. In *International Conference on Learning Representations (ICLR)*, 2018.
- [4] Bach, S., Binder, A., Montavon, G., Klauschen, F., Müller, K.-R., and Samek, W. On pixel-wise explanations for non-linear classifier decisions by layer-wise relevance propagation. *PloS one*, 10(7):e0130140, 2015.
- [5] Bau, D., Zhou, B., Khosla, A., Oliva, A., and Torralba, A. Network dissection: Quantifying interpretability of deep visual representations. *IEEE Transactions on Pattern Analysis and Machine Intelligence (TPAMI)*, pp. 6541–6549, 2017.
- [6] Bossard, L., Guillaumin, M., and Van Gool, L. Food-101—mining discriminative components with random forests. In *Proceedings of the European Conference on Computer Vision (ECCV)*, pp. 446–461. Springer, 2014.
- [7] Chattopadhyay, A., Sarkar, A., Howlader, P., and Balasubramanian, V. N. Grad-cam++: Generalized gradient-based visual explanations for deep convolutional networks. In *2018 IEEE Winter Conference on Applications of Computer Vision (WACV)*, pp. 839–847. IEEE, 2018.
- [8] Chen, X., Liu, C., Li, B., Lu, K., and Song, D. Targeted backdoor attacks on deep learning systems using data poisoning. *arXiv preprint arXiv:1712.05526*, 2017.
- [9] Chen, Y., Li, J., Xiao, H., Jin, X., Yan, S., and Feng, J. Dual path networks. In *Advances in Neural Information Processing Systems (NeurIPS)*, pp. 4467–4475, 2017.
- [10] Chollet, F. Xception: Deep learning with depthwise separable convolutions. In *IEEE Conference on Computer Vision and Pattern Recognition (CVPR)*, pp. 1251–1258, 2017.
- [11] Deng, J., Dong, W., Socher, R., Li, L.-J., Li, K., and Fei-Fei, L. Imagenet: A large-scale hierarchical image database. In *IEEE Conference on Computer Vision and Pattern Recognition (CVPR)*, pp. 248–255, 2009.
- [12] Ding, X., Guo, Y., Ding, G., and Han, J. Acnet: Strengthening the kernel skeletons for powerful cnn via asymmetric convolution blocks. In *IEEE Conference on Computer Vision and Pattern Recognition (CVPR)*, pp. 1911–1920, 2019.
- [13] Doshi-Velez, F. and Kim, B. Towards a rigorous science of interpretable machine learning. *arXiv preprint arXiv:1702.08608*, 2017.
- [14] Gao, S., Cheng, M.-M., Zhao, K., Zhang, X.-Y., Yang, M.-H., and Torr, P. H. Res2net: A new multi-scale backbone architecture. 2019.
- [15] Gu, T., Dolan-Gavitt, B., and Garg, S. Badnets: Identifying vulnerabilities in the machine learning model supply chain. *arXiv preprint arXiv:1708.06733*, 2017.
- [16] He, K., Zhang, X., Ren, S., and Sun, J. Deep residual learning for image recognition. In *IEEE Conference on Computer Vision and Pattern Recognition (CVPR)*, 2016.
- [17] Hooker, S., Erhan, D., Kindermans, P.-J., and Kim, B. A benchmark for interpretability methods in deep neural networks. In *Advances in Neural Information Processing Systems (NeurIPS)*, pp. 9737–9748, 2019.

- [18] Howard, A., Sandler, M., Chu, G., Chen, L.-C., Chen, B., Tan, M., Wang, W., Zhu, Y., Pang, R., Vasudevan, V., et al. Searching for mobilenetv3. In *IEEE Conference on Computer Vision and Pattern Recognition (CVPR)*, 2019.
- [19] Howard, A. G., Zhu, M., Chen, B., Kalenichenko, D., Wang, W., Weyand, T., Andreetto, M., and Adam, H. Mobilenets: Efficient convolutional neural networks for mobile vision applications. *arXiv preprint arXiv:1704.04861*, 2017.
- [20] Hu, J., Shen, L., and Sun, G. Squeeze-and-excitation networks. In *IEEE Conference on Computer Vision and Pattern Recognition (CVPR)*, 2018.
- [21] Huang, G., Liu, Z., Van Der Maaten, L., and Weinberger, K. Q. Densely connected convolutional networks. In *IEEE Conference on Computer Vision and Pattern Recognition (CVPR)*, pp. 4700–4708, 2017.
- [22] Iandola, F. N., Han, S., Moskewicz, M. W., Ashraf, K., Dally, W. J., and Keutzer, K. Squeezenet: Alexnet-level accuracy with 50x fewer parameters and < 0.5 mb model size. *arXiv preprint arXiv:1602.07360*, 2016.
- [23] Jeyakumar, J. V., Noor, J., Cheng, Y.-H., Garcia, L., and Srivastava, M. How can i explain this to you? an empirical study of deep neural network explanation methods. In *Advances in Neural Information Processing Systems (NeurIPS)*, 2020.
- [24] Koh, P. W. and Liang, P. Understanding black-box predictions via influence functions. In *International Conference on Machine Learning (ICML)*, pp. 1885–1894. PMLR, 2017.
- [25] Krause, J., Stark, M., Deng, J., and Fei-Fei, L. 3D object representations for fine-grained categorization. In *IEEE Conference on Computer Vision and Pattern Recognition (CVPR)*, pp. 554–561, 2013.
- [26] Krizhevsky, A., Sutskever, I., and Hinton, G. E. Imagenet classification with deep convolutional neural networks. In *Advances in Neural Information Processing Systems (NeurIPS)*, 2012.
- [27] Lage, I., Chen, E., He, J., Narayanan, M., Kim, B., Gershman, S., and Doshi-Velez, F. An evaluation of the human-interpretability of explanation. *arXiv preprint arXiv:1902.00006*, 2019.
- [28] Lin, T.-Y., Maire, M., Belongie, S., Hays, J., Perona, P., Ramanan, D., Dollár, P., and Zitnick, C. L. Microsoft coco: Common objects in context. In *Proceedings of the European Conference on Computer Vision (ECCV)*, pp. 740–755. Springer, 2014.
- [29] Lin, Y.-S., Lee, W.-C., and Celik, Z. B. What do you see? evaluation of explainable artificial intelligence (xai) interpretability through neural backdoors. *arXiv preprint arXiv:2009.10639*, 2020.
- [30] Liu, H., Simonyan, K., and Yang, Y. Darts: Differentiable architecture search. *arXiv preprint arXiv:1806.09055*, 2018.
- [31] Lundberg, S. M. and Lee, S.-I. A unified approach to interpreting model predictions. In *Advances in Neural Information Processing Systems (NeurIPS)*, pp. 4765–4774, 2017.
- [32] Ma, N., Zhang, X., Zheng, H.-T., and Sun, J. Shufflenet v2: Practical guidelines for efficient cnn architecture design. In *Proceedings of the European Conference on Computer Vision (ECCV)*, pp. 116–131, 2018.
- [33] Nilsback, M.-E. and Zisserman, A. Automated flower classification over a large number of classes. In *Sixth Indian Conference on Computer Vision, Graphics & Image Processing*, pp. 722–729. IEEE, 2008.
- [34] Petsiuk, V., Das, A., and Saenko, K. Rise: Randomized input sampling for explanation of black-box models. In *Proceedings of the British Machine Vision Conference (BMVC)*, 2018.
- [35] Redmon, J. and Farhadi, A. Yolov3: An incremental improvement. *arXiv preprint arXiv:1804.02767*, 2018.

- [36] Redmon, J., Divvala, S., Girshick, R., and Farhadi, A. You only look once: Unified, real-time object detection. In *IEEE Conference on Computer Vision and Pattern Recognition (CVPR)*, pp. 779–788, 2016.
- [37] Ribeiro, M. T., Singh, S., and Guestrin, C. "why should i trust you?" explaining the predictions of any classifier. In *Proceedings of the 22nd ACM SIGKDD international conference on knowledge discovery and data mining*, pp. 1135–1144, 2016.
- [38] Samek, W., Binder, A., Montavon, G., Lapuschkin, S., and Müller, K.-R. Evaluating the visualization of what a deep neural network has learned. *IEEE transactions on neural networks and learning systems*, 28(11):2660–2673, 2016.
- [39] Sandler, M., Howard, A., Zhu, M., Zhmoginov, A., and Chen, L.-C. Mobilenetv2: Inverted residuals and linear bottlenecks. In *IEEE Conference on Computer Vision and Pattern Recognition (CVPR)*, 2018.
- [40] Selvaraju, R. R., Cogswell, M., Das, A., Vedantam, R., Parikh, D., and Batra, D. Grad-cam: Visual explanations from deep networks via gradient-based localization. *International Journal of Computer Vision (IJCV)*, 128(2):336–359, 2020.
- [41] Sermanet, P., Eigen, D., Zhang, X., Mathieu, M., Fergus, R., and LeCun, Y. Overfeat: Integrated recognition, localization and detection using convolutional networks. In *International Conference on Learning Representations (ICLR)*, 2014.
- [42] Shrikumar, A., Greenside, P., and Kundaje, A. Learning important features through propagating activation differences. In *International Conference on Machine Learning (ICML)*, pp. 3145–3153, 2017.
- [43] Simonyan, K. and Zisserman, A. Very deep convolutional networks for large-scale image recognition. In *International Conference on Learning Representations (ICLR)*, 2015.
- [44] Smilkov, D., Thorat, N., Kim, B., Viégas, F., and Wattenberg, M. Smoothgrad: removing noise by adding noise. In *ICML Workshop on Visualization for Deep Learning*, 2017.
- [45] Sundararajan, M., Taly, A., and Yan, Q. Axiomatic attribution for deep networks. In *International Conference on Machine Learning (ICML)*, 2017.
- [46] Szegedy, C., Liu, W., Jia, Y., Sermanet, P., Reed, S., Anguelov, D., Erhan, D., Vanhoucke, V., and Rabinovich, A. Going deeper with convolutions. In *IEEE Conference on Computer Vision and Pattern Recognition (CVPR)*, pp. 1–9, 2015.
- [47] Tan, M. and Le, Q. V. Efficientnet: Rethinking model scaling for convolutional neural networks. In *International Conference on Machine Learning (ICML)*, 2019.
- [48] van der Linden, I., Haned, H., and Kanoulas, E. Global aggregations of local explanations for black box models. *FACTS-IR: Fairness, Accountability, Confidentiality, Transparency, and Safety - SIGIR 2019 Workshop*, 2019.
- [49] Vedaldi, A. and Soatto, S. Quick shift and kernel methods for mode seeking. In *Proceedings of the European Conference on Computer Vision (ECCV)*, pp. 705–718. Springer, 2008.
- [50] Vu, M. N., Nguyen, T. D., Phan, N., Gera, R., and Thai, M. T. Evaluating explainers via perturbation. *arXiv preprint arXiv:1906.02032*, 2019.
- [51] Wang, H., Wang, Z., Du, M., Yang, F., Zhang, Z., Ding, S., Mardziel, P., and Hu, X. Score-cam: Score-weighted visual explanations for convolutional neural networks. In *Proceedings of the IEEE/CVF Conference on Computer Vision and Pattern Recognition Workshops*, pp. 24–25, 2020.
- [52] Wang, J., Sun, K., Cheng, T., Jiang, B., Deng, C., Zhao, Y., Liu, D., Mu, Y., Tan, M., Wang, X., et al. Deep high-resolution representation learning for visual recognition. 2020.
- [53] Welinder, P., Branson, S., Mita, T., Wah, C., Schroff, F., Belongie, S., and Perona, P. Caltech-UCSD birds 200. Technical Report CNS-TR-2010-001, California Institute of Technology, 2010.

- [54] Xie, S., Girshick, R., Dollár, P., Tu, Z., and He, K. Aggregated residual transformations for deep neural networks. In *IEEE Conference on Computer Vision and Pattern Recognition (CVPR)*, 2017.
- [55] Yang, M. and Kim, B. Benchmarking attribution methods with relative feature importance. *arXiv*, pp. arXiv-1907, 2019.
- [56] Yeh, C.-K., Hsieh, C.-Y., Suggala, A. S., Inouye, D. I., and Ravikumar, P. On the (in) fidelity and sensitivity for explanations. In *Advances in neural information processing systems (NeurIPS)*, 2019.
- [57] Zhang, Q., Yang, Y., Ma, H., and Wu, Y. N. Interpreting cnns via decision trees. In *IEEE Conference on Computer Vision and Pattern Recognition (CVPR)*, pp. 6261–6270, 2019.
- [58] Zhang, X., Zhou, X., Lin, M., and Sun, J. Shufflenet: An extremely efficient convolutional neural network for mobile devices. In *IEEE Conference on Computer Vision and Pattern Recognition (CVPR)*, 2018.
- [59] Zhou, B., Khosla, A., Lapedriza, A., Oliva, A., and Torralba, A. Learning deep features for discriminative localization. In *IEEE Conference on Computer Vision and Pattern Recognition (CVPR)*, pp. 2921–2929, 2016.

A Complete Pseudocode of Cross-Model Consensus of Explanations

In the main text, Algorithm 1 presents the pseudocode of our framework of Cross-Model Consensus of Explanations. Here, Algorithm 2 completes the pseudocode of the framework with the details of the three functions that are used in Algorithm 1.

Algorithm 2: Functions in Algorithm 1.

```

1 Function interpret ( $\mathcal{A}$ ,  $d$ ,  $M$ ):
   /* An interpretation algorithm  $\mathcal{A}$ , a data sample  $d$  and a trained model  $M$ . */
2   return Explanation result of  $M$  on  $d$  by  $\mathcal{A}$ .
3 Function reach_consensus( $L$ ):
   /*  $L$ , a collection of interpretations of  $m$  models for one given data sample. */
4   return  $c$ , the consensus of the interpretations of  $m$  models:  $c_k = \frac{1}{m} \sum_{i=1}^m \frac{L_{ik}^2}{\|L_i\|}$  for LIME
   explanations;  $c_k = \frac{1}{m} \sum_{i=1}^m \frac{L_{ik} - \min(L_i)}{\max(L_i) - \min(L_i)}$  for SmoothGrad explanations.
5 Function similarity( $a$ ,  $b$ ):
   /* Two vectors  $a$  and  $b$ . */
6   return The similarity score between  $a$  and  $b$ :  $s = \frac{\langle a, b \rangle}{\|a\| \|b\|}$  for LIME interpretations;
    $s = e^{-\frac{(\|a-b\|/\sigma)^2}{2}}$  for SmoothGrad interpretations.
```

B Experimental Details

In this section, we present technique details of the experiments in the main text about the preparation of deep models for committee formations, the interpretation algorithms and the user-study evaluations.

B.1 Committee Formations

There are around 100 deep models trained on ImageNet that are publicly available² at the moment we initiate the experiments. We first exclude some very large models that take much more computation resources. Then for the consistency of computing superpixels, we include only the models that take images of size 224×224 as input, resulting 81 models for the committee based on ImageNet. For the intentions of comparing the models, a solution to including the models in the committee is to simply align the superpixels in different sizes of images. However, in our experiments, we choose not to do so since there are already a large number of available models.

As for CUB-200-2011 [53], similarly we first exclude the very large models. Then we follow the standard procedures [41, 43] for fine-tuning ImageNet-pretrained models on CUB-200-2011. For simplicity, we use the same training setup for fine-tuning all pre-trained models on CUB-200-2011 (learning rate 0.01, batch size 64, SGD optimizer with momentum 0.9, resize to 256 being the short edge, randomly cropping images to the size of 224×224), and obtain 85 models that are well trained. Different hyper-parameters may help to improve the performance of some specific networks, but for the same reason of the large number of available models, we choose not to search for better hyper-parameter settings.

For Stanford Cars 196 [25], Oxford Flowers 102 [33] and Foods 101 [6], we follow the same fine-tuning procedure as on CUB-200-2011. However, given the convergence over committee sizes (Figure 6), which suggests a committee of more than 15 models, we randomly choose around 20 models for each of the three datasets.

B.2 Interpretation Algorithms

To explain a deep model’s predictions, LIME [37] on vision tasks first performs a superpixel segmentation [49] for an image, then generates interpolated samples by randomly masking some superpixels and computing the outputs of the generated samples through the model, and finally fits the model

²https://github.com/PaddlePaddle/models/blob/release/1.8/PaddleCV/image_classification/README_en.md#supported-models-and-performances

outputs with the presence/absence of superpixels as input by a linear regression model. The linear weights then directly indicates the feature importance in superpixel level as the explanation result.

The gradients of model output w.r.t. input can partly identify influential pixels, but due to the saturation of activation functions in the deep networks, the vanilla gradient is usually noisy. SmoothGrad [44] reduces the visual noise by repeatedly adding small random noises to the input so as to get a list of corresponding gradients, which are then averaged for the final explanation result.

Note that many other interpretation algorithms are also available for our proposed framework while in this paper, we validate our approach with two trustworthy and commonly-used algorithms.

B.3 Human User-Study Evaluations

As introduced in the main text, we have conducted user-study experiments for model interpretability over the five models that are discussed by Network Dissection, i.e., DenseNet161, ResNet152, VGG16, GoogLeNet, AlexNet, and the evaluation result from user-study evaluations well aligns with results of our framework using either LIME or SmoothGrad. We describe here the experimental settings of the user-study evaluations.

For each image, we randomly choose two models from the five models and present the LIME (or SmoothGrad respectively) explanations of the two models, without giving the model information to users. Users are then requested to choose which one helps better to reveal the model’s reasoning of making predictions according to their understanding, or equal if the two interpretations are equally bad or good. Each pair of models is repeated three times and represented to different users. The better one in each pair will get three points and the other one will get zero; in the equal case, both get one point. Finally, a normalization of dividing the number of images and the number of repeats (i.e. 3) is performed for each model. The user-study evaluations yield the scores indicating the model interpretability, as shown in Table 1.

C ResNet Family

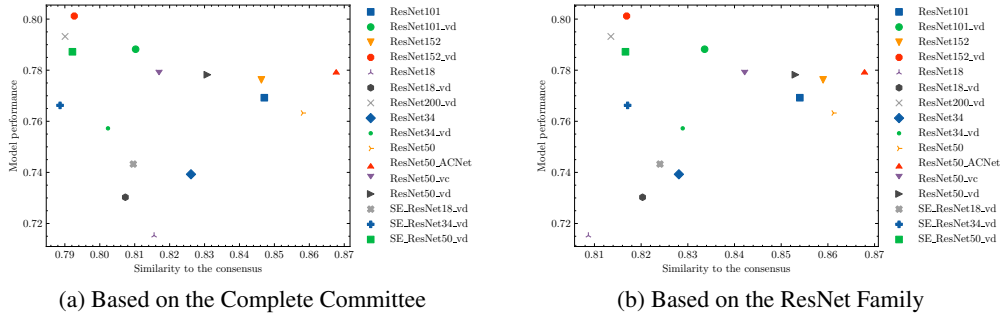


Figure 9: Model performance v.s. similarity to the consensus of LIME on ResNet family. The consensus of (a) is voted by the complete committee on ImageNet (81 models), while the consensus of (b) is voted by ResNet family (16 models).

We show the zoomed plot of ResNet family (whose name contains “ResNet” key word) in the ImageNet-LIME committee of 81 models in Figure 9 (a). Meanwhile, we also present the results using ResNet family as committee in Figure 9 (b). These two subfigures have no large difference, which further confirms the consistency of our approach across different committees for ranking models. The positive correlation between the model performance and the consensus scores does not exist in the ResNet family, as we explained before that in some local areas, especially when models are extremely large, the correlation is not always positive.

D References of Network Structures

Most frequently-used structures of deep models have been evaluated in this paper, including AlexNet [26], ResNet [16], ResNeXt [54], SEResNet [20], ShuffleNet [58, 32], MobileNet [19, 39, 18], VGG

[43], GoogleNet [46], Inception [46], Xception [10], DarkNet [36, 35], DenseNet [21], DPN [9], SqueezeNet [22], EfficientNet [47], Res2Net [14], HRNet [52], Darts [30], AcNet [12] and their variants.

E Numerical Report of Main Plots

Due to the large number of deep models evaluated, Figure 8, Figure 4 and Figure 5 grouped some that are of the same architecture. Here, we report all of the corresponding numerical results in Table 2 with a smaller scale.

F More Visualization Results

We present more visualization results of cross-model consensus of explanations in Figure 10, Figure 11, Figure 12 and Figure 13, where the samples are from ImageNet and CUB-200-2011.

For further explorations, we visualize several random images from MS-COCO [28], shown in Figure 14. As introduced in Section 5, one direction for the future work would extend the proposed framework on the datasets with multiple visual objects and complicated background for object detection, segmentation, and multi-label classification tasks.

Table 2: Numerical report of model performance and similarity to the consensus using LIME and SmoothGrad over 81 models on ImageNet in sub-table(a) corresponding to Figure 5 (a, b, c), and over 85 models on CUB-200-2011 in sub-table(b) corresponding to Figure 4, 8 and 5 (d, e, f).

(a) on ImageNet				(b) on CUB-200-2011					
	perf.	Consensus Scores w/ LIME	Consensus Scores w/ Smooth-Grad		perf.	Consensus Scores w/ LIME	Consensus Scores w/ Smooth-Grad	mAP between g.t. of segmentation and LIME explanation	mAP between g.t. of segmentation and SmoothGrad explanation
AlexNet	0.575	0.594	0.0214	AlexNet	0.507	0.536	0.0275	0.343	0.571
AutoDL_4M	0.752	0.756	0.0312	AutoDL_4M	0.728	0.781	0.0371	0.594	0.693
AutoDL_6M	0.776	0.741	0.0291	AutoDL_6M	0.754	0.811	0.0402	0.605	0.740
DPN107	0.798	0.828	0.0331	DPN107	0.830	0.867	0.0525	0.630	0.780
DPN131	0.802	0.833	0.0334	DPN131	0.800	0.868	0.0498	0.643	0.795
DPN68	0.766	0.849	0.0297	DPN68	0.795	0.849	0.0415	0.630	0.710
DPN92	0.775	0.845	0.0357	DPN92	0.806	0.872	0.0510	0.626	0.784
DPN98	0.798	0.837	0.0354	DPN98	0.815	0.877	0.0526	0.628	0.793
DenseNet121	0.755	0.859	0.0376	DenseNet163_ImageNet1k	0.782	0.850	0.0485	0.604	0.743
DenseNet161	0.781	0.849	0.0383	DenseNet121	0.771	0.848	0.0503	0.585	0.771
DenseNet169	0.765	0.855	0.0376	DenseNet161	0.813	0.873	0.0542	0.640	0.797
DenseNet201	0.779	0.843	0.0385	DenseNet169	0.792	0.858	0.0513	0.609	0.776
DenseNet264	0.761	0.841	0.0378	DenseNet201	0.805	0.858	0.0544	0.616	0.795
EfficientNetB0	0.754	0.727	0.0355	DenseNet264	0.789	0.868	0.0540	0.628	0.798
EfficientNetB0_Small	0.708	0.729	0.0362	EfficientNetB0	0.765	0.805	0.0450	0.594	0.769
GoogleNet	0.726	0.734	0.0260	EfficientNetB0_Small	0.737	0.805	0.0426	0.589	0.738
HRNet_W18_C	0.766	0.854	0.0388	EfficientNetB1	0.775	0.805	0.0456	0.593	0.755
HRNet_W30_C	0.776	0.832	0.0378	EfficientNetB2	0.787	0.819	0.0461	0.595	0.764
HRNet_W32_C	0.781	0.845	0.0376	EfficientNetB3	0.791	0.812	0.0421	0.582	0.771
HRNet_W40_C	0.773	0.822	0.0366	EfficientNetB4	0.792	0.829	0.0423	0.612	0.766
HRNet_W44_C	0.782	0.817	0.0368	EfficientNetB5	0.774	0.808	0.0431	0.591	0.768
HRNet_W48_C	0.794	0.807	0.0369	HRNet_W18_C	0.754	0.831	0.0461	0.592	0.736
HRNet_W64_C	0.784	0.799	0.0344	HRNet_W30_C	0.770	0.832	0.0475	0.595	0.752
MobileNetV1	0.711	0.825	0.0322	HRNet_W32_C	0.785	0.836	0.0471	0.586	0.750
MobileNetV1_x0_25	0.513	0.653	0.0222	HRNet_W40_C	0.750	0.844	0.0476	0.594	0.763
MobileNetV1_x0_5	0.640	0.751	0.0257	HRNet_W44_C	0.788	0.830	0.0449	0.592	0.752
MobileNetV1_x0_75	0.697	0.788	0.0297	HRNet_W48_C	0.796	0.838	0.0482	0.581	0.757
MobileNetV2	0.742	0.812	0.0342	HRNet_W64_C	0.791	0.838	0.0485	0.609	0.766
MobileNetV2_x0_25	0.534	0.650	0.0221	InceptionV4	0.745	0.797	0.0435	0.592	0.728
MobileNetV2_x0_5	0.642	0.768	0.0270	MobileNetV1	0.741	0.824	0.0415	0.588	0.716
MobileNetV2_x0_75	0.709	0.795	0.0302	MobileNetV1_x0_25	0.557	0.676	0.0288	0.448	0.634
MobileNetV2_x1_5	0.737	0.841	0.0336	MobileNetV1_x0_5	0.655	0.753	0.0325	0.527	0.672
MobileNetV2_x2_0	0.744	0.840	0.0352	MobileNetV1_x0_75	0.688	0.808	0.0388	0.569	0.701
Res2Net101_vd_26w_4s	0.780	0.752	0.0285	MobileNetV2	0.737	0.810	0.0438	0.582	0.732
Res2Net50_14w_8s	0.781	0.823	0.0324	MobileNetV2_x0_25	0.511	0.670	0.0287	0.457	0.597
Res2Net50_26w_4s	0.780	0.835	0.0343	MobileNetV2_x0_5	0.665	0.753	0.0337	0.543	0.661
Res2Net50_vd_26w_4s	0.790	0.828	0.0332	MobileNetV2_x0_75	0.715	0.814	0.0369	0.577	0.686
ResNeXt101_32x4d	0.784	0.843	0.0371	MobileNetV2_x1_5	0.756	0.835	0.0421	0.611	0.719
ResNeXt101_vd_32x4d	0.795	0.830	0.0347	MobileNetV2_x2_0	0.781	0.851	0.0425	0.605	0.705
ResNeXt101_vd_64x4d	0.784	0.821	0.0336	Res2Net101_vd_26w_4s	0.799	0.853	0.0470	0.613	0.756
ResNeXt152_32x4d	0.782	0.842	0.0377	Res2Net50_14w_8s	0.789	0.826	0.0491	0.587	0.765
ResNeXt152_64x4d	0.787	0.828	0.0383	Res2Net50_26w_4s	0.768	0.840	0.0515	0.601	0.782
ResNeXt152_vd_32x4d	0.792	0.807	0.0325	Res2Net50_vd_26w_4s	0.783	0.821	0.0467	0.604	0.749
ResNeXt152_vd_64x4d	0.790	0.814	0.0325	ResNeXt101_32x4d	0.818	0.877	0.0578	0.629	0.798
ResNeXt50_32x4d	0.765	0.849	0.0385	ResNeXt101_32x8d_wsl	0.768	0.831	0.0479	0.563	0.755
ResNeXt50_64x4d	0.784	0.836	0.0389	ResNeXt101_vd_32x4d	0.816	0.867	0.0494	0.614	0.771
ResNeXt50_vd_32x4d	0.790	0.844	0.0346	ResNeXt101_vd_64x4d	0.824	0.871	0.0520	0.642	0.778
ResNeXt50_vd_64x4d	0.792	0.829	0.0360	ResNeXt152_32x4d	0.815	0.872	0.0543	0.619	0.792
ResNet101	0.769	0.847	0.0377	ResNeXt152_64x4d	0.834	0.875	0.0576	0.613	0.779
ResNet101_vd	0.788	0.810	0.0323	ResNeXt152_vd_32x4d	0.820	0.872	0.0520	0.640	0.788
ResNet152	0.776	0.846	0.0374	ResNeXt152_vd_64x4d	0.822	0.852	0.0479	0.618	0.764
ResNet152_vd	0.801	0.793	0.0308	ResNeXt50_32x4d	0.809	0.856	0.0567	0.619	0.785
ResNet18	0.715	0.816	0.0342	ResNeXt50_64x4d	0.814	0.885	0.0562	0.621	0.788
ResNet18_vd	0.730	0.807	0.0334	ResNeXt50_vd_32x4d	0.806	0.874	0.0508	0.627	0.762
ResNet200_vd	0.793	0.790	0.0300	ResNeXt50_vd_64x4d	0.820	0.890	0.0544	0.631	0.785
ResNet34	0.739	0.826	0.0363	ResNet101	0.784	0.878	0.0511	0.620	0.761
ResNet34_vd	0.757	0.802	0.0329	ResNet101_vd	0.813	0.864	0.0499	0.606	0.766
ResNet50	0.763	0.858	0.0394	ResNet152	0.799	0.859	0.0506	0.601	0.773
ResNet50_ACNet	0.780	0.868	0.0386	ResNet152_vd	0.797	0.851	0.0507	0.613	0.774
ResNet50_vc	0.778	0.817	0.0370	ResNet18	0.726	0.794	0.0449	0.546	0.735
ResNet50_vd	0.778	0.831	0.0341	ResNet18_vd	0.754	0.846	0.0428	0.598	0.710
SENet154_vd	0.803	0.807	0.0315	ResNet200_vd	0.813	0.861	0.0502	0.618	0.773
SE_ResNeXt101_32x4d	0.781	0.818	0.0325	ResNet34	0.758	0.812	0.0461	0.569	0.756
SE_ResNeXt50_32x4d	0.775	0.810	0.0321	ResNet34_vd	0.771	0.833	0.0435	0.570	0.731
SE_ResNeXt50_vd_32x4d	0.797	0.819	0.0342	ResNet50	0.776	0.878	0.0531	0.609	0.774
SE_ResNet18_vd	0.743	0.810	0.0342	ResNet50_ACNet	0.782	0.870	0.0481	0.619	0.737
SE_ResNet34_vd	0.766	0.789	0.0330	ResNet50_vd	0.795	0.876	0.0461	0.634	0.741
SE_ResNet50_vd	0.787	0.792	0.0332	SE_ResNeXt101_32x4d	0.793	0.838	0.0452	0.605	0.750
ShuffleNetV2	0.706	0.795	0.0325	SE_ResNeXt50_32x4d	0.798	0.821	0.0438	0.578	0.727
ShuffleNetV2_x0_25	0.507	0.636	0.0231	SE_ResNeXt50_vd_32x4d	0.799	0.863	0.0479	0.617	0.729
ShuffleNetV2_x0_33	0.547	0.651	0.0238	SE_ResNet18_vd	0.727	0.802	0.0396	0.550	0.673
ShuffleNetV2_x0_5	0.611	0.710	0.0250	SE_ResNet34_vd	0.754	0.803	0.0450	0.574	0.731
ShuffleNetV2_x1_0	0.689	0.778	0.0295	SE_ResNet50_vd	0.771	0.870	0.0446	0.616	0.732
ShuffleNetV2_x1_5	0.712	0.807	0.0306	ShuffleNetV2	0.696	0.817	0.0375	0.571	0.668
ShuffleNetV2_x2_0	0.738	0.816	0.0317	ShuffleNetV2_x0_25	0.519	0.687	0.0263	0.448	0.563
SqueezeNet1_0	0.602	0.732	0.0253	ShuffleNetV2_x0_33	0.530	0.686	0.0294	0.465	0.622
SqueezeNet1_1	0.613	0.762	0.0242	ShuffleNetV2_x0_5	0.605	0.753	0.0307	0.500	0.624
VGG11	0.694	0.801	0.0291	ShuffleNetV2_x1_0	0.695	0.788	0.0354	0.564	0.667
VGG13	0.697	0.804	0.0297	ShuffleNetV2_x1_5	0.728	0.815	0.0371	0.564	0.670
VGG16	0.714	0.821	0.0305	ShuffleNetV2_x2_0	0.731	0.806	0.0402	0.574	0.683
VGG19	0.722	0.821	0.0309	Xception41	0.801	0.833	0.0501	0.605	0.761
				Xception41_deepab	0.775	0.753	0.0412	0.559	0.734
				Xception65	0.801	0.837	0.0479	0.609	0.740
				Xception65_deepab	0.747	0.800	0.0415	0.586	0.728
				Xception71	0.775	0.846	0.0479	0.613	0.760
				consensus	0.859	N/A	N/A	0.704	0.818



Figure 10: More visual comparisons between the consensus and the explanations of deep models with LIME on samples from ImageNet. Note that the consensus (last column) is the cross-model consensus of explanations.

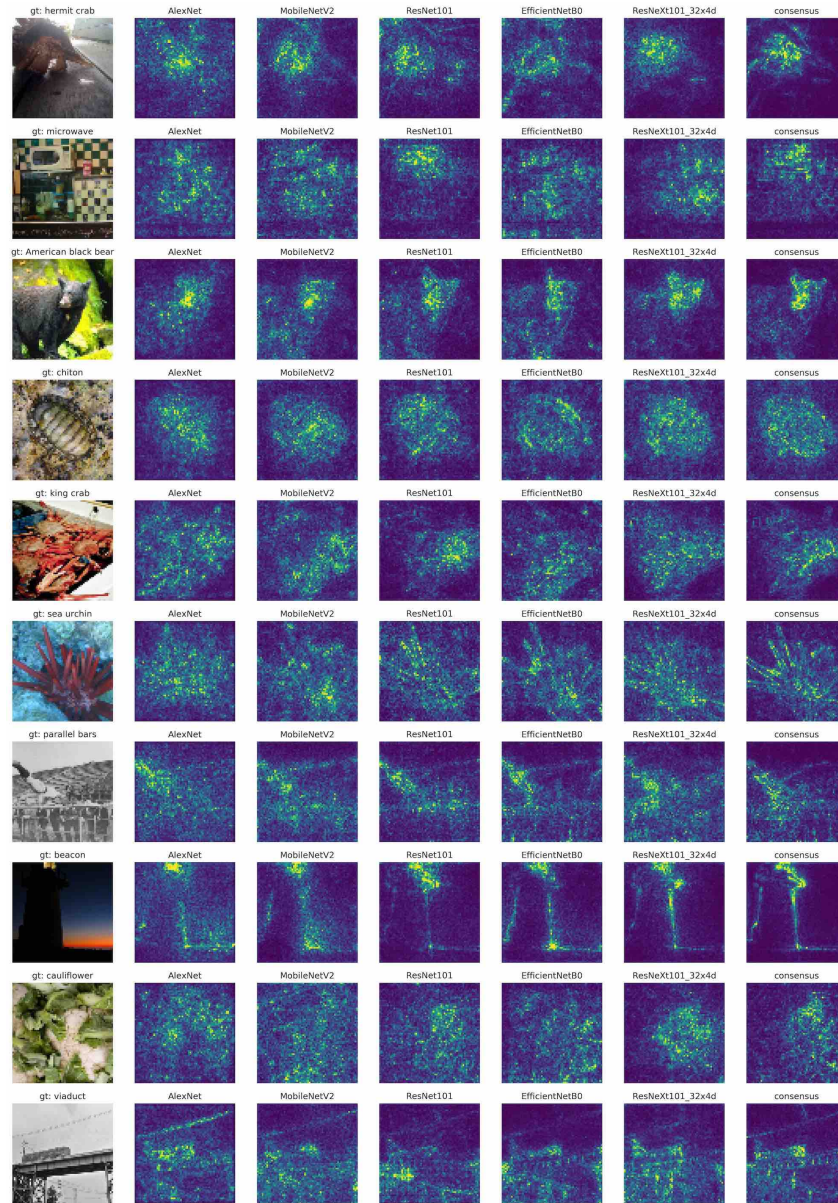


Figure 11: More visual comparisons between the consensus and the explanations of deep models with SmoothGrad on samples from ImageNet. Note that the consensus (last column) is the cross-model consensus of explanations.

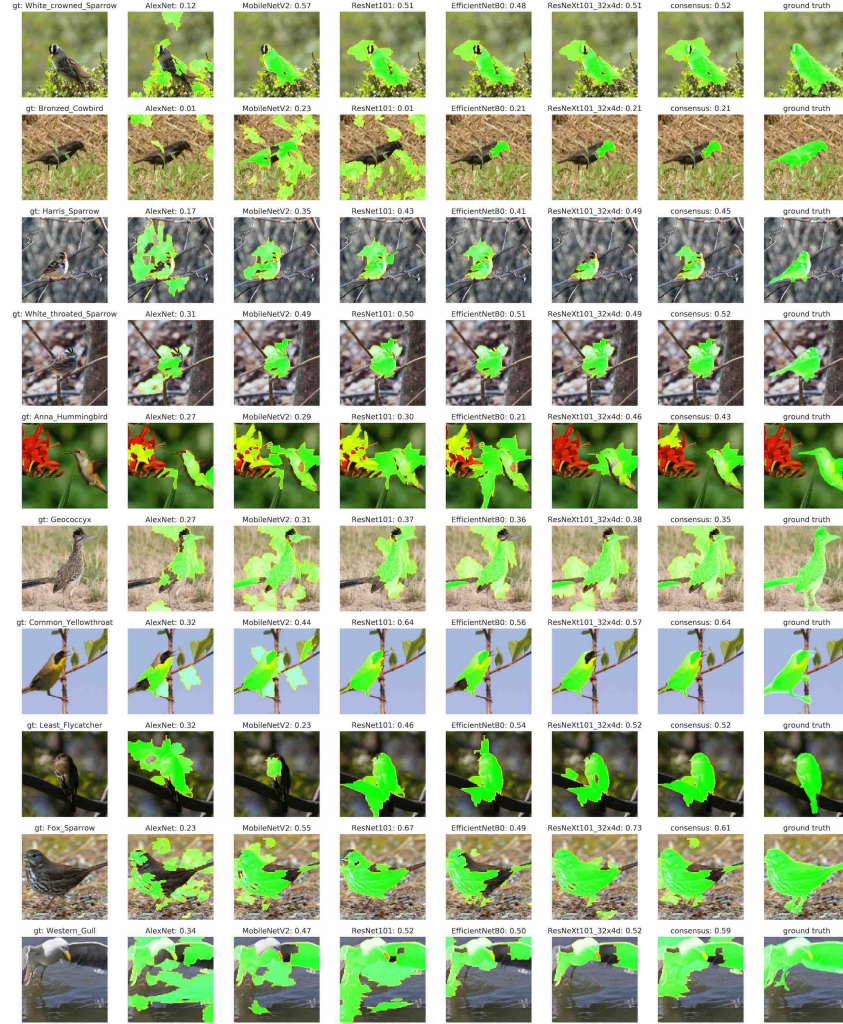


Figure 12: More visual comparisons between the consensus and the explanations of deep models with LIME on samples from CUB-200-2011, where the pixel-wise annotations of image segmentation are available and the mAPs are measured for the similarity to the segmentation ground truth. Note that the consensus (second last column) is the cross-model consensus of explanations.

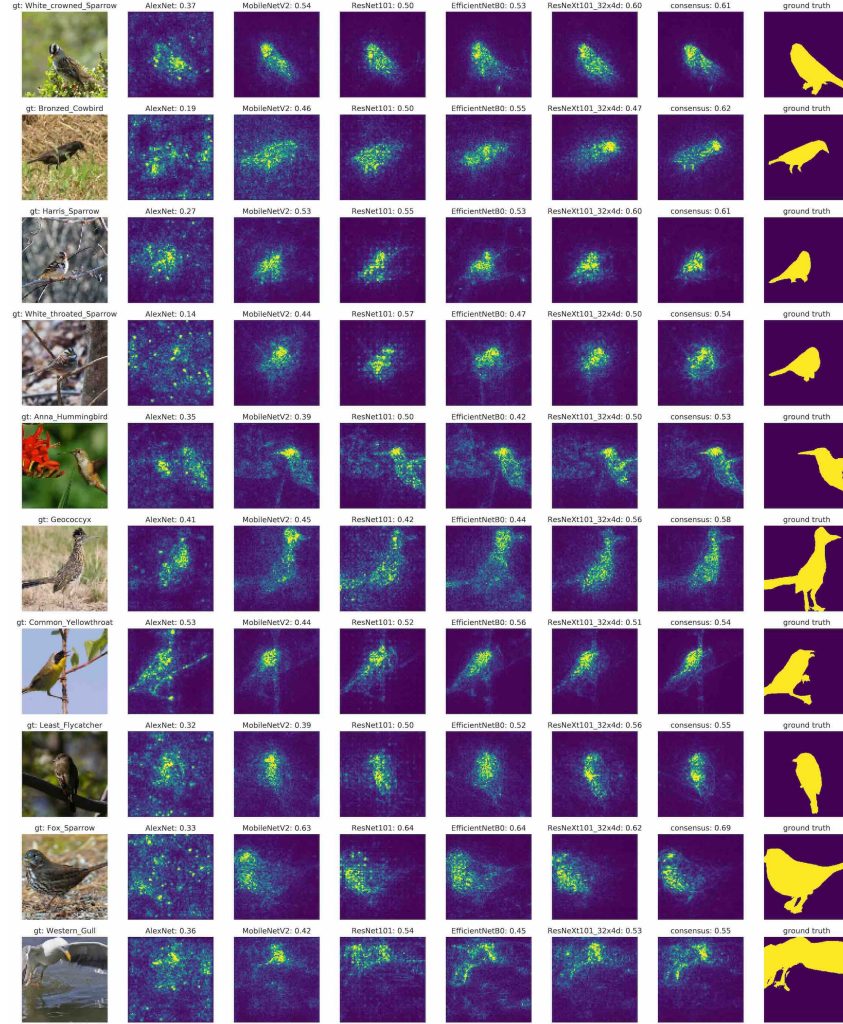


Figure 13: More visual comparisons between the consensus and the explanations of deep models with SmoothGrad on samples from CUB-200-2011, where the pixel-wise annotations of image segmentation are available and the mAPs are measured for the similarity to the segmentation ground truth. Note that the consensus (second last column) is the cross-model consensus of explanations.

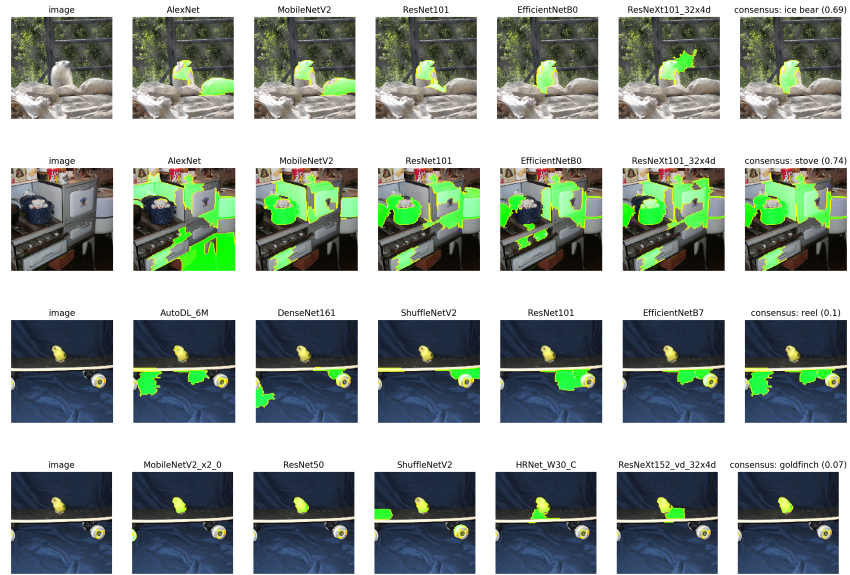


Figure 14: Visualization of images from the MS-COCO dataset [28] for showing the potentials of cross-model consensus of explanations, where the predicted label with probability is noted.